Engineering Innovations
ISSN: 2813-1002, Vol. 4, pp 1-8
doi:10.4028/p-391e5g

Submitted: 2022-06-20
Accepted: 2022-06-21
Online: 2023-02-15

Finite Element Analysis of Damage of Cylindrical Roller Bearing of Main Shaft of Shot Blasting Machine

Zhang Yijia[1,a], Pan Yongzhi[1,b], Jiang Zhengfeng[2,c], Fu Xiuli[1,d*], Zhang Tianyi[1,e]

[1]School of Mechanical Engineering, University of Jinan, China

[2]Zibo TAA Metal Technology Co., Ltd., China

[a]2541616354@qq.com, [b]me_panyz@ujn.edu.cn, [c]1685784494@qq.com, [d]me_fuxl@ujn.edu.cn, [e]1364711071@qq.com

Keywords: Shot blasting machine; Cylindrical roller bearing; Thermal-structural coupling; Damage; The finite element

Abstract. The main shaft of shot blasting machine mainly uses cylindrical roller bearing as the supporting part. The influence of stress, strain and temperature on bearing damage was studied by thermal-structural coupling analysis of the bearing through finite element simulation. The causes and main damage forms of bearing surface were verified by super depth of field observation and finite element analysis. It is found that there exists pyramidal strain in the contact area between inner and outer raceway and roller, and its distribution form is continuous point distribution. The stress concentration is mainly distributed in the contact area between the roller face and the retaining edge, and the roller temperature is more concentrated in the area near the end face. The maximum length and depth of spalling pit on racetrack surface were 572.2μm and 14.15μm respectively. The maximum width and depth of the scratches on the roller surface are 386.7μm and 10.7μm, and the damage degree of the roller surface is not uniform. The thermo-structural coupling analysis is used to simulate the running state of bearings, which is of guiding significance to analyze the failure forms of bearings and improve the service life of bearings.

Introduction

Cylindrical roller bearings are widely used in manufacturing preparation because of their large bearing capacity and high speed and heavy load conditions[1-2]. Through modern finite element analysis, the bearing structure is constantly optimized, and the service life and performance of bearings are constantly improved[3]. Bearing performance is directly related to the use of the spindle system, and has a direct impact on the stability and reliability of the whole equipment[4]. Therefore, as far as possible to reduce bearing damage in the process of use, improve the service life has been the focus of research in the industry.

The main shaft of the shot blasting machine uses a pair of cylindrical roller bearings as the main support. Problems such as skidding, heating up and vibration will occur during the use of the main bearing, which will inevitably cause some damage or even failure to the bearing. Studies have found that about 60%-70% of bearing failures are caused by fatigue. Many scholars at home and abroad have conducted extensive studies on bearing dynamics and statics, and conducted thermal-structural coupling analysis of bearings through finite element to explore the causes of bearing failures[5].

In this paper, the main shaft cylindrical roller bearing NU2218E of shot blasting machine is taken as the research object. The finite element simulation analysis of the bearing was carried out according to the working condition to study the influence of the bearing heat and force on the damage under the working condition.

Analysis of Motion State of Cylindrical Roller Bearing

The research on the motion state of cylindrical roller bearing requires the hypothesis analysis of the motion mode of roller. It is assumed that the bearing roller only has pure rolling in the motion

process and has good contact with the inner and outer rings, and the contact mode is linear contact. Bearing inner ring angular velocity is ω; The rotational angular velocity of the roller is ω_τ; The roller rotates at an angular velocity of ω_r, which is opposite to the angular velocity of revolution. F is the radial load of the bearing, F_r is the radial load of the roller, and $F_r\cos n\varphi$ is the reaction force of the radial force F. Figure 1a shows the motion state of the bearing.

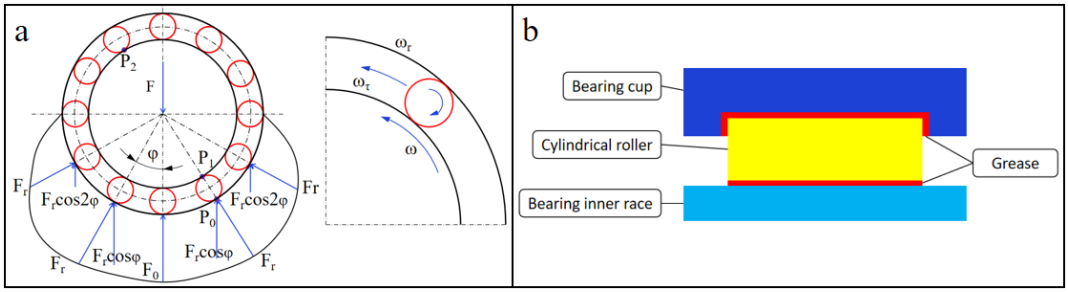

Fig. 1 Bearing motion state diagram (a) and thermal structure model (b)

During the installation process, there is a certain gap between the roller and the inner ring. After loading, the contact point of the lower roller and the inner ring is P_1 and the contact point of the outer ring is P_0. The contact point of the upper roller is P_2. When the roller moves to the bottom of the bearing chamber, it receives the maximum radial force F_0. According to formula 1.1, the maximum radial force F_0 on the roller can be calculated

$$F_0 = \frac{4.08}{Z} F \tag{1}$$

Where: F -- radial force received by the bearing; Z -- number of rollers. Formula 1.1 is the contact force of bearing line.

Under the action of radial force reaction force Frcosnφ, the roller is subjected to tangential component force, and the roller rotation line speed does not match the inner ring line speed. The bearing roller is filled with grease between the inner and outer rings. If F_0 is too large, the thickness of the oil film will decrease and the friction force will increase. Bearing heat mainly comes from the heating of roller stirring grease and the collision and friction between roller and inner and outer raceway. The heat generated by the bearing forms thermal convection through the grease, and the heat is transmitted to the inner and outer rings for heat conduction and outward diffusion. Figure 1b is the bearing thermal structure model diagram.

Bearing friction power loss is converted into heat, and power loss mainly depends on friction torque. Part of the friction torque is determined by the material and speed

$$M_0 = 10^{-7} f_0 (vn)^{\frac{2}{3}} d_m^{\ 3} \qquad vn \geq 2000 \tag{2}$$

$$M_0 = 160 \times 10^{-7} f_0 d_m^{\ 3} \qquad vn < 2000 \tag{3}$$

Where: d_m -- bearing section circle diameter, ㎜; f_0 -- Coefficient related to bearing type and lubrication mode, take f_0 =3; n -- Bearing speed, take n=2400r/min; v -- Kinematic viscosity of lubricant, take v =2.8mm2/s.

The other part of the friction torque is determined by the load

$$M_1 = f_1 P_1 d_m \tag{4}$$

Where: f_1 -- coefficient related to load, f1=0.00045; P_1 -- Load on bearing, N.

The total friction torque can be simplified as

$$M = M_0 + M_1 \tag{5}$$

The power loss caused by friction heat can be calculated by the friction torque

$$N = 1.05 \times 10^{-4} nM \tag{6}$$

Through calculation, the power loss of single roller is 68.14W.

Finite Element Analysis

3D modeling. The three-dimensional model of NU2218E cylindrical roller bearing was established by using finite element software. The specific design parameters of the bearing were shown in Figurre 2, and the other modeling parameters were obtained by measuring the entity. In the modeling process, chamfering, fillet and cage are omitted to simplify the model calculation. Three-dimensional bearing model is shown in Figurre 2.

Parameter	Numerical value	Parameter	Numerical value
Outer diameter of outer ring/mm	160	Roller diameter/mm	19
Inner diameter of outer ring/mm	145	Roller width/mm	28
Outer diameter of inner ring/mm	107	Number of rollers	17
Inner diameter of inner ring/mm	45	Bearing width/mm	40

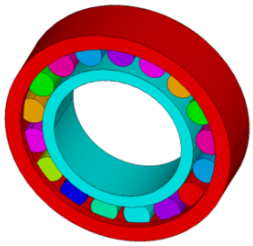

Fig. 2 NU2218E 3D model and design parameters

Define unit and material parameters. Bearing steel has high hardness and large elastic modulus. Common grades are GCr6, GCr15, G20CrMo and so on. The internal diffusion of heat in the bearing is complicated. Solid unit Solid226 and surface effect unit Surf152 are selected for structural thermal analysis. Solid226 is a 20-node, 6-degree-of-freedom solid unit with hybrid analysis capabilities for elastic deformation analysis of incompressible materials. The Surf152 is mainly used for various 3D thermal analysis and can be superimposed on any thermal cell surface. GCr15 was selected as the bearing material for analysis, and the material parameters are shown in Table 1.

Table 1 GCr15 material parameter table[6]

Parameter	Numerical value			
Temperature/°C	20	100	200	300
Density/ (kg· m^3)	7791.8	7766.7	7737.8	7706.8
Modulus of elasticity/ MPa	2.13×10^5	2.07×10^5	2.01×10^5	1.95×10^5
Poisson's ratio	0.3	0.3	0.3	0.3
Thermal conductivity/ ($W\cdot m^{-1}\cdot K^{-1}$)	35.62	39.05	39.36	37.76
Specific heat/ ($J\cdot kg^{-1}\cdot K^{-1}$)	477.63	491.46	505.12	525.46
Coefficient of thermal expansion/ K^{-1}	10.23×10^{-6}	10.72×10^{-6}	11.54×10^{-6}	12.11×10^{-6}

Meshing, establishing contact pairs and surface effect elements. The outer ring, roller and inner ring of the bearing are meshed respectively. The grid length is set to 0.0024m, and the grid shape is triangular, which can be meshed freely. A total of 281302 units and 337094 nodes were established. Ten mutually independent contact working surfaces, including inner surface, outer surface, inner raceway, outer raceway, front and rear guard edge, front and rear end face of roller, upper and lower surface of roller, were selected, and the surface effect units were established successively. A total of 10 surface effect units were established. Contact pairs were selected, and contact pairs were established for outer raceway-outer surface of roller, inner raceway-inner surface of roller and front and rear fenders -bearing end face. The contact mode was face-surface contact, and a total of 4 contact pairs were established. Figure 3 is a schematic diagram of meshing, surface effect unit and contact pair.

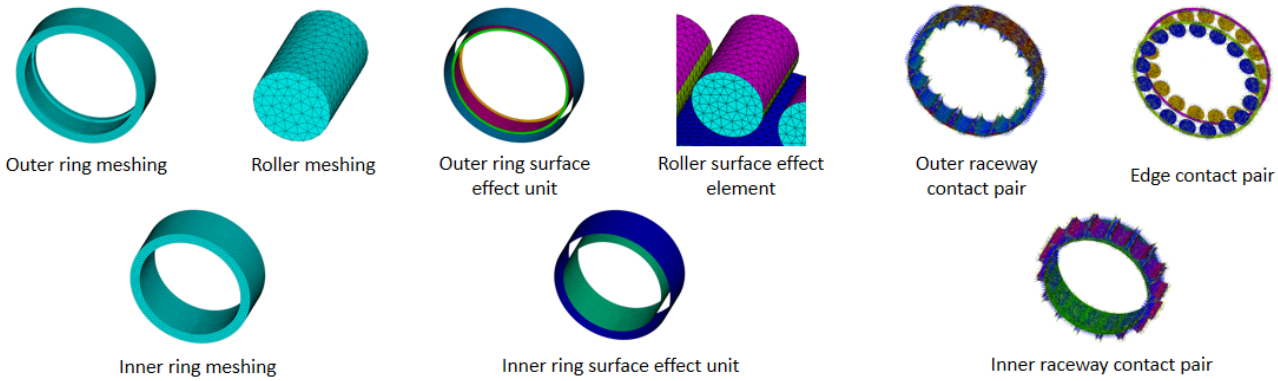

Fig. 3 Schematic diagram of meshing, surface effect unit and contact pair

Apply boundary conditions. Bearing is complicated in the actual running process, so it needs to be simplified and analyzed as an ideal model. The rotation speed of the shot blasting machine will be affected by the load, so the spindle angular speed is 252rad/s. When the spindle is running at high speed, the main load comes from the rotating shaft and the impeller. It is assumed that the spindle is subjected to a fixed load F in the normal operation, with a vertical downward direction and a magnitude of 1000N. The initial temperature applied to the outermost ring is 20℃, the initial temperature applied to the innermost ring is 80℃, and the initial temperature increases successively from the outermost ring to the innermost ring. In the cylindrical coordinate system, the bearing outer ring is stationary, and all nodes on the outer surface of the bearing outer ring are fully constrained. The inner ring of the bearing can only rotate axially due to the limitation of the main shaft, and the X-axis and Z-axis constraints are imposed on the nodes on the inner surface of the inner ring. The roller is restricted by the inner and outer ring and the guard edge can only rotate and revolution. The X-axis constraint is imposed on the circular surface node of the roller, and the Z-axis constraint is imposed on the end node of the roller. Figure 4 is a schematic diagram of bearing boundary conditions.

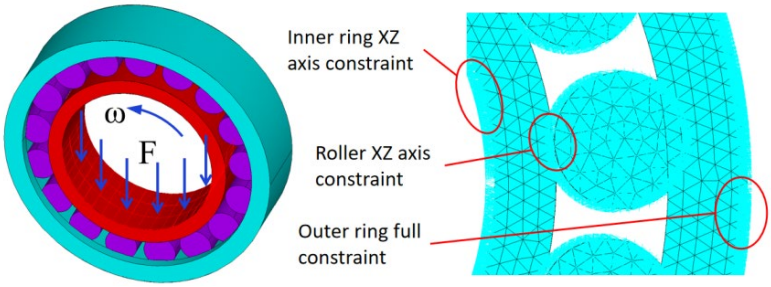

Fig. 4 Schematic diagram of boundary conditions

Analysis of Simulation Results

Stress analysis. The results show that the surface of the outer raceway, roller and inner raceway has many spot-like protrusions, the strain of outer ring retaining edge is outward, and the strain of roller face is different degree. Because the force acts vertically on the vertical direction of the contact line between the roller and the raceway, the surface of the contact line is subjected to compression deformation, and the material around the contact line is subjected to a certain degree of tensile stress, resulting in tensile deformation[7]. At the same time, due to the temperature rise, the bearing parts produce thermal expansion, which further increases the contact stress between the roller and the outer raceway, and adversely affects the oil film between the roller and the raceway in the operation process. As a result, the force element of the outer raceway is subjected to repeated tensile/compressive stress, and the surface is subjected to periodic tensile/compressive elastic deformation, and a spot-like strain area is formed. Figure 5 is the bearing strain cloud diagram.

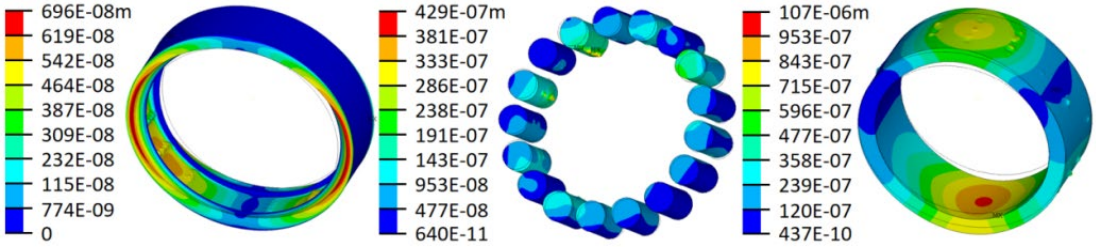

Fig. 5 Cloud diagram of bearing strain

The stress at the outer rim of the ring is distributed at intervals, the stress at both ends of the roller is more concentrated, and the stress on the inner pipe surface is arranged neatly and distributed in strips. Roller high-speed operation produces a lot of friction heat, resulting in the expansion of the roller heat caused by extrusion of the retaining edge. At the same time, the "edge effect" leads to the stress concentration at both ends of the roller, which forces the elastic deformation at both ends of the roller to be larger than the middle area[8]. The above reasons cause stress concentration in the contact area between the retaining edge and the roller face. It can be seen from Figure 6 that the deformation of roller end face and retaining edge is not uniform, and the contact state is complex surface contact, which aggravates the friction and wear of working surface. Figure 6 is the bearing stress cloud diagram.

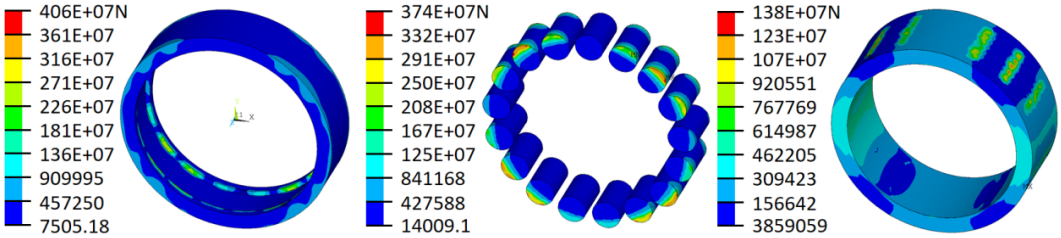

Fig. 6 Cloud diagram of bearing stress

Temperature field analysis. The bearing temperature gradually decreases from the outer surface to the inner surface. The highest roller temperature is the contact area between the roller and the outer raceway, and the temperature at both ends of the roller is higher than the middle area. The temperature gradient between the outer raceway and the roller, and between the roller and the raceway is large, which is caused by the different movement speed of grease in the bearing cavity. With the increasing bearing temperature and height, the viscosity coefficient of grease decreases continuously, and the effective bearing oil layer cannot be formed between roller and raceway, resulting in the increase of friction between roller and raceway. The load of the main shaft of the shot blasting machine is not stable in the working process, which leads to the bearing will be affected by impact and vibration in the operation process, and skid and rub injury occurs[9-10]. The temperature of contact area between roller and raceway increases sharply due to skid and scratch injury, and the temperature rise of outer raceway is obviously higher than that of inner raceway. Figure 7 is the bearing temperature cloud diagram.

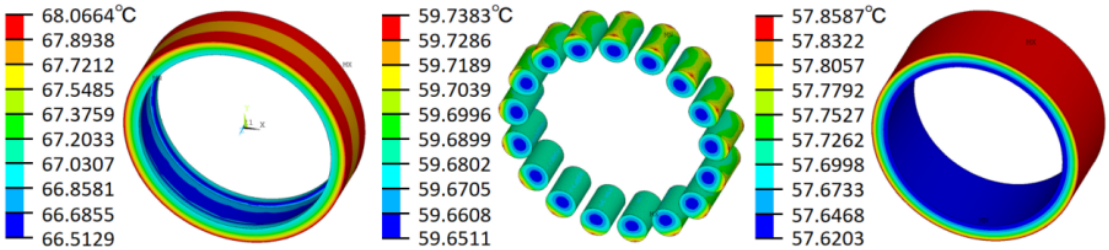

Fig. 7 Cloud chart of bearing temperature

Damage Verification

Cylindrical roller bearings include outer ring, inner ring, roller and cage. Different degrees of friction will occur between roller and inner raceway, roller and outer raceway, roller end face and rim in the process of bearing operation.

Compared with the undamaged raceway surface, the spalling pits of different sizes are not evenly distributed on the damaged raceway surface, and the spalling area is mainly concentrated in the middle of the raceway, which is consistent with the regular strain band composed of point strains on the raceway surface outside the strain cloud map. In some areas of the outer ring retaining edge, there are scratches distributed along the direction of roller movement. As can be seen from the stress-strain cloud diagram, the strain on the retaining edge is large along the symmetrical direction of the central axis, and the indirect stress is concentrated along the circumferential direction of the bearing. The two ends of the cylindrical roller are trimmed during the manufacturing process to increase the fatigue resistance of the roller[3]. Roller at both ends of the arc slope (bright belt) there is about 18mm wide wear area, distribution of irregular ribbons and scratches. Comparing the cloud images, it is found that there are high temperature and stress concentration in the area with severe roller scratches. Figure 8 Comparison of damage of roller bearings.

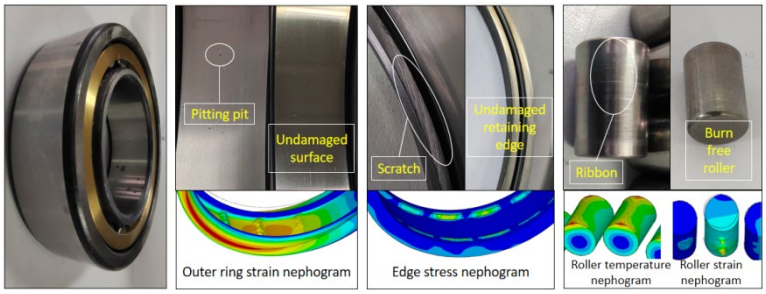

Fig. 8 Damage comparison diagram of various parts of roller bearing

Through the ultra depth of field equipment can intuitively observe the damage, respectively at the outer raceway spalling pit and roller surface observation. Select the concave area of the outer raceway for super depth of field observation, it can observe the obvious spalling pit, the location of the concave pit and the surrounding area have an obvious height difference, and the concave pit is relatively gentle, the edge of the irregular fracture zone. The section was observed in 45° direction of the pit. The length of the section was 572.2μm, and the maximum depth was 14.15μm. Figure 9 is a super depth of field view of the outer raceway surface.

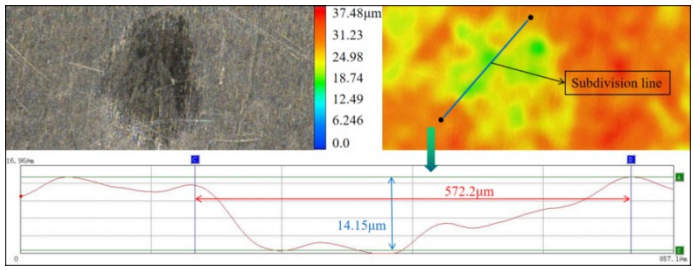

Fig. 9 Observation of super depth of field on inner raceway surface

Select the roller with color band for observation. There is obvious color difference on the roller surface, and there are many peeling pits and scratches. Two parallel lines M and N were selected on the adjacent position of the roller surface. The maximum width and depth of the scratches on the selected position were 386.7μm and 10.7μm respectively. And M, N two lines have obvious height difference, which indicates that the roller surface damage degree is not uniform, there are different degrees of pits and different depths of scratch. Figure 10 shows super depth of field observation of roller surface.

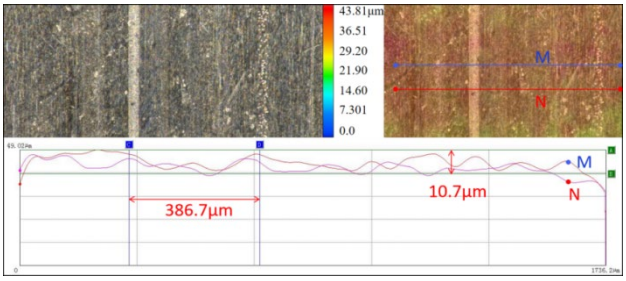

Fig. 10 Observation of super depth of field on roller surface

Bearing in the use of poor heat dissipation, temperature difference between the two parts is too large, large thermal deformation and local stress concentration will produce scratches, scratches and overheating damage, with the increase of the use of time, damage intensification, slowly developed into burns, scratches and peeling[11]. There are many spalling pits on the surface of the raceway due to the alternating load in the process of use, and the main damage form is fatigue pitting. After the roller deformation under load and thermal expansion deformation, there is a large pressure on the edge of the guard, resulting in the stress concentration of the edge of the guard, a large strain, the main form of damage is scratch. Under the working environment of 57-59℃, the viscosity coefficient of grease decreases, and the oil film with effective bearing capacity cannot be formed. Its lubrication and protection effect is weakened, leading to direct contact and relative sliding between roller and inner and outer raceway. At the same time, the instantaneous temperature of roller surface is too high due to the flash temperature effect caused by skidding, and the damage form is mainly burn, scratch and pitting.

Summary

Due to the limitation of finite element analysis, the mesh is divided by triangles freely and the solid element is a hexahedron model. Because the contact area between roller and raceway is very small, great contact stress and strain are produced, which leads to some errors in the analysis results. Applying boundary conditions closer to actual working conditions and reducing analysis errors will be the next key task. Through the structural thermal analysis of the cylindrical roller bearing NU2218E, the following conclusions are drawn:

(1)Bearing in the process of use will produce high temperature, roller and outer raceway contact area temperature is greater than the inner raceway contact area, which is consistent with the fact that the damage degree of the outer ring is greater than the inner ring.

(2)The inner and outer raceway surfaces are subjected to periodic tension and compression stress, and the strain of each part of the bearing appears in the finite element analysis similar to pyramid shape.

(3)There are obvious spalling pits on the outer ring surface. There are scratches and spalling pits on the surface of the roller, and the scratches are not consistent in the circumference of the roller depth; The edge of the guard is severely scratched under high stress.

References

[1] Jin Qianchong, Zhang Qing, Luo Jun, Xie Xiangyu, Xu Jin. Bearing, 2019 (12): 39-43

[2] Yang Fan, Xu Kefeng. Harbin bearing, 2020,41 (03): 19-22

[3] Xu Mingqi, Zheng Hongwei, Qu Qiong. Bearing, 2014 (08): 28-31

[4] Chen Jiaqing, Zhang Pei, Xu Linlin. Journal of Beijing Institute of petrochemical technology, 2001 (01): 32-38

[5] Jia Dongsheng, Zhang min. Journal of Zhejiang Vocational and Technical College of industry and commerce, 2010,9 (04): 82-83 + 88

[6] Song Nan. Jilin University, 2017

[7] Liu Jinchao, Wang Chengguo. China Railway Science, 2002 (02): 86-94

[8] Chen Jiaqing, Zhang Pei, Xu Linlin. Journal of Beijing Institute of petrochemical technology, 2001 (01): 32-38

[9] Fowell M, Ioannides S, Kadiric A. Tribology Transactions, 2014, 57(3): 472-488.

[10] Li J, Chen W, Xie Y. Proceedings of the Institution of Mechanical Engineers, Part J: Journal of Engineering Tribology, 2014, 228(10): 1036-1046.

[11] Li Haiqi, Yang Xu. Fan technology, 2008 (06): 78-80